Discrete time translation symmetry breaking in a Josephson junction laser

Ben Lang, Grace F. Morley, and Andrew D. Armour
School of Physics and Astronomy and Centre for the Mathematics and Theoretical Physics of Quantum Non-Equilibrium Systems, University of Nottingham, Nottingham NG7 2RD, United Kingdom

(Received 12 August 2022; revised 6 April 2023; accepted 6 April 2023; published 21 April 2023)

A Josephson junction laser is realized when a microwave cavity is driven by a voltage-biased Josephson junction. Through the ac Josephson effect, a dc voltage generates a periodic drive that acts on the cavity and generates interactions between its modes. A sufficiently strong drive enables processes that downconvert a drive resonant with a high harmonic into photons at the cavity fundamental frequency, breaking the discrete time translation symmetry set by the Josephson frequency. Using a classical model, we determine when and how this transition occurs as a function of the bias voltage and the number of cavity modes. We find that certain combinations of mode number and voltage tend to facilitate the transition which emerges via an instability within a subset of the modes. Despite the complexity of the system, there are cases in which the critical drive strength can be obtained analytically.

DOI: 10.1103/PhysRevB.107.144509

I. INTRODUCTION

Circuit QED systems are ideally suited to the exploration of nonlinear phenomena, such as frequency conversion, which underlie the breaking of discrete time translational symmetries [1–3]. Famously, applying a dc voltage, V, to an isolated Josephson junction (JJ) leads to oscillations at the Josephson frequency, $\omega_J = 2eV/\hbar$. However, if the junction is embedded in a microwave cavity, interactions between the strongly nonlinear junction and cavity modes can trigger oscillations at frequencies below ω_J, breaking the discrete time-translational symmetry (DTTS). The resulting downconversion processes and the properties of the radiation they generate have been widely explored in few mode systems over the last few years, both experimentally [4–7] and theoretically [8–12].

The breaking of a DTTS has been studied extensively elsewhere in the context of many-body systems of coupled oscillators and the symmetry broken time-crystalline phases that emerge [13–17]. For superconducting circuits, although attention has largely focused on systems where just one or two modes play an important role, the possibilities enabled by utilizing multiple modes are attracting increasing attention [18]. In particular, recent experiments revealed strong coherent radiation at the fundamental mode frequency in a JJ-cavity system where ω_J matched a high overtone of the cavity [19]. In this system, known as a Josephson junction laser (JJL) [19,20], emission at the fundamental mode frequency is believed to result from an interplay between many of the cavity's modes [19]. Inspired by the JJL experiments, in this paper we analyze a simplified theoretical model of a voltage-biased JJ in series with a cavity, described as a set of N harmonic modes [see Fig. 1(a)]. We explore the many-body discrete time-translational symmetry breaking (DTTSB) transition which manifests as a change in the periodicity of the cavity oscillations [see Fig 1(b)]: from $2\pi/\omega_J$ to a larger value set by the period of the fundamental mode. Numerical modeling has highlighted the crucial role played by the multiple modes supported by the cavity [19] and a solution obtained analytically for the time-crystal-like symmetry-broken regime [20]. However, the fundamental questions we seek to answer of when and how the transition occurs have not been addressed.

The JJ leads to a Hamiltonian which ostensibly generates all-to-all couplings between cavity modes, but most of these couplings are irrelevant as they are far off-resonant. Adopting a rotating wave approximation (RWA) and a coherent state ansatz, we find that, prior to the transition, the modes fall into noninteracting subspaces with different symmetry properties. This division into subspaces means that the location of the DTTSB transition proves surprisingly dependent on the number of cavity modes. Relatively low transition thresholds are associated with cases where the transition is continuous, and we demonstrate that in such cases it initially arises from an instability affecting modes in a single subspace. Remarkably, closed form expressions for the critical coupling can be obtained in some cases.

II. MODEL SYSTEM

The JJL can be modeled as a set of harmonic cavity modes in series with a JJ to which a dc voltage bias V is applied [19–23]. The phase across the JJ is controlled by the voltage and contributions from each of the modes leading to a Hamiltonian [21,22,24–26],

$$\hat{H}(t) = \sum_n \hbar\omega_n \hat{a}_n^\dagger \hat{a}_n - E_J \cos\left[\omega_J t + \sum_n \Delta_n(\hat{a}_n^\dagger + \hat{a}_n)\right], \tag{1}$$

where E_J is the Josephson energy of the junction, $\hat{a}_n$ is the raising operator for the nth cavity mode with frequency ω_n, and $\Delta_n = \sqrt{2e^2/(\hbar C\omega_n)}$ is the corresponding strength of the zero point flux fluctuations (in units of the flux quantum) with C the cavity capacitance [21]. Here, the JJ phase is locked to the sum of the time-dependent contribution from the voltage, $\omega_J t$, and the flux across each of the modes, $\sum_n \Delta_n(\hat{a}_n^\dagger + \hat{a}_n)$, see, e.g., Ref. [21] for a detailed derivation. The Hamiltonian possesses the DTTS, $\hat{H}(t) = \hat{H}(t + T_J)$ with period $T_J = 2\pi/\omega_J$.

The explicit time dependence of the cosine term in the Hamiltonian Eq. (1) acts as a nonlinear drive whose strength can be tuned by varying E_J [19,21]. This term is balanced by dissipation, since photons can leak out of the cavity into its surroundings. Assuming zero temperature for simplicity, the dissipation can be described via a standard Lindblad master equation [22,24,25,27,28]

$$\dot{\rho} = -\frac{\mathrm{i}}{\hbar}[\hat{H}(t), \rho] + \sum_n \frac{\gamma_n}{2}(2\hat{a}_n\rho\hat{a}_n^\dagger - \hat{a}_n^\dagger\hat{a}_n\rho - \rho\hat{a}_n^\dagger\hat{a}_n), \quad (2)$$

with γ_n the loss rate for mode n.

In the following, we assume a hard cutoff in the number of modes, N, together with an idealized cavity spectrum, $\omega_n = n\omega_1$, where ω_1 is the fundamental mode frequency, and a constant loss rate $\gamma_n = \gamma$ [19,20]. In practice, deviations in the mode frequencies and changes to the damping rate will eventually become important as the mode index is increased [21,29], leading to an effective decoupling of high frequency modes, but how this occurs will depend on precisely how the JJL is engineered. Rather than concentrate on a single specific realization, we will consider the simplest case: a hard cutoff that treats N as a parameter, allowing us to focus on exploring how it affects the location and character of the DTTSB transition. However, we will also consider the extent to which our methods and findings apply more generally to cases where the cutoff in the number of modes is no longer sharp but rather occurs gradually because of a smooth increase in the damping rate with mode index (Appendix C).

III. CLASSICAL DYNAMICS

We analyze the classical dynamics of the system using a coherent state ansatz to derive an approximate set of coupled classical equations for the mode amplitudes [30]. We assume that each mode is in a coherent state, $\rho_\alpha = \bigotimes_{n=1}^N |\alpha_n\rangle\langle\alpha_n|$, with α_n a complex time-dependent amplitude [21,30]. This approach is a variant on the standard semiclassical approximation technique of taking expectation values of Heisenberg equations of motion and then replacing expectations of operator products by the corresponding product of expectation values (see, e.g., Ref. [31]). It is most accurate when the nonlinearity is sufficiently weak that it only becomes relevant for large photon numbers. This corresponds to low values of Δ_1, and indeed $\Delta_1 \to 0$ constitutes the classical limit for the system [11,32]. The classical equations of motion obtained in this way also provide a framework which is typically very helpful in developing an analysis of the full quantum problem, while also serving as a starting point for approximate descriptions of the role of quantum fluctuations [11,21,30–32].

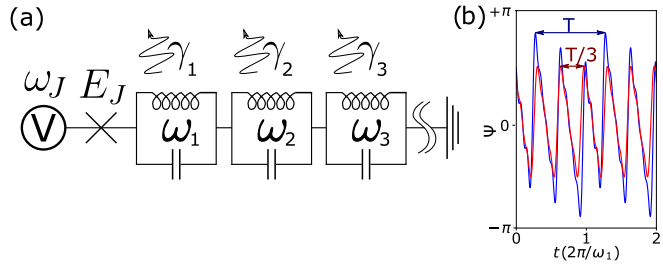

FIG. 1. (a) Circuit model of the JJL. A JJ with Josephson energy, E_J, biased by a voltage, V, in series with a microwave cavity modeled as a series of LC oscillators with frequencies $\omega_1, \omega_2, \ldots$. Losses from the cavity lead to damping of the modes with rates $\gamma_1, \gamma_2, \ldots$. (b) DTTS breaking transition in the oscillations of the total cavity phase, $\Psi(t)$: Above the transition (blue), these have the period of the fundamental mode, $T = 2\pi/\omega_1$, but period $2\pi/\omega_J$ below (red). Here, $N = 11$, $\omega_J = 3\omega_1$, and the origin of the time axis has been displaced to display the long-time behavior clearly.

The corresponding classical Hamiltonian $\mathcal{H}(t, \vec{\alpha})$ is obtained from its quantum counterpart [Eq. (1)] by making the replacements $\hat{a}_n^{(\dagger)} \to \alpha_n^{(*)}$ and $E_J \to \tilde{E}_J = E_J \exp[-\frac{1}{2}\sum_{n=1}^N \Delta_n^2]$ (this arises when normal ordering is performed) [6,21,33–35]. Combined with Eq. (2), this leads to dynamical equations for the amplitudes of the form

$$\dot{\alpha}_n = -\left(\mathrm{i}\omega_n + \frac{\gamma}{2}\right)\alpha_n - \frac{\mathrm{i}\tilde{E}_J\Delta_n}{\hbar}\sin(\omega_J t + \Psi), \quad (3)$$

where $\Psi = 2\sum_n \Delta_n \mathrm{Re}[\alpha_n]$ is the total phase across all of the modes [20].

To identify the transition, the equations for the amplitudes are integrated numerically. We focus on the case where the drive is resonant with a higher harmonic $\omega_J = p\omega_1$ ($p = 2, 3, \ldots$) and vary the dimensionless drive strength [20] $\lambda = \tilde{E}_J\Delta_1^2/\hbar\gamma$. At very weak drives, excitation starts in the resonant mode ($\omega_p = p\omega_1 = \omega_J$), but the cosine term in the Hamiltonian Eq. (1) upconverts these oscillations into effective drives at $m\omega_J$ (with m a positive integer), progressively exciting the resonant harmonics—all those modes with frequencies matching $m\omega_J$. The transition occurs when the excitation spreads beyond the resonant harmonics—it is seen clearly in the behavior of Ψ which changes from a sawtooth oscillation of period $T_J = 2\pi/\omega_J$ in the symmetry-preserving phase to one with period $T_1 = 2\pi/\omega_1$ when the symmetry is broken [Fig. 1(b)].

Tracing the response of the individual mode amplitudes reveals that the transition can be either continuous or discontinuous (see Fig. 2), depending on the precise relationship between N and p. Surprisingly, Fig. 2 shows that changing N by just one can trigger a change from a continuous to discontinuous transition accompanied by a large increase in the critical coupling.

IV. CONTINUOUS TRANSITIONS

To understand the connections between the characteristics of the transition and the properties of the system, we now focus on analyzing cases where a continuous transition occurs. In such cases, important simplifications can be made

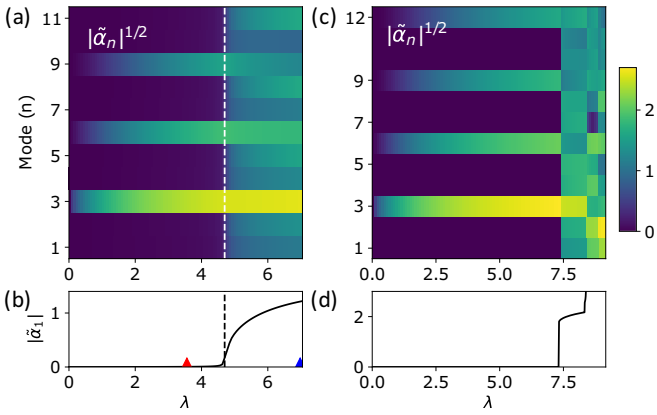

FIG. 2. Long-time behavior of $\tilde{\alpha}_n$, the component of α_n oscillating at ω_n, as a function of λ with $p = 3$ for $N = 11$ (a), (b)—a continuous transition–and $N = 12$ (c), (d)—a discontinuous transition. In both cases, $\Delta_1 = 0.2$ and $\gamma = \omega_1/100$. (a), (c) show $|\tilde{\alpha}_n|$ for all modes; (b), (d) show just the fundamental, $|\tilde{\alpha}_1|$, which serves as an order parameter for the transition. See Appendix A for details of the numerical method. Red and blue symbols in (b) indicate the λ values illustrated in Fig. 1(b). The vertical dashed lines show the threshold predicted using linear stability analysis.

which allow approximate analytic methods to be employed so the transition can be located without the need for numerical integration.

The first simplification is obtained by making a RWA [6,21,30,34]. Assuming $\omega_J = p\omega_1 + \delta$, with δ a small detuning, we move to a rotating frame by applying the transformation

$$\hat{U}(t) = \exp\left(\mathrm{i}\sum_{n=1}^{N} n(\omega_J/p)\,\hat{a}_n^\dagger \hat{a}_n\, t\right). \tag{4}$$

The RWA is made by discarding nonresonant processes so each mode is assumed to oscillate only at is own frequency [36]. The resulting Hamiltonian can be written

$$\hat{H}_{\mathrm{RWA}} = \sum_{n=1}^{N} \hbar\delta_n \hat{a}_n^\dagger \hat{a}_n - \frac{\tilde{E}_J}{2}\left[Z_p^{\{N\}}(\vec{\hat{x}}) + \mathrm{H.c.}\right], \tag{5}$$

where $\delta_n = -(n/p)\delta$, $\vec{\hat{x}} = (\hat{x}_1, \ldots, \hat{x}_N)$ with $\hat{x}_n = 2\mathrm{i}\Delta_n \hat{a}_n$, and we have defined

$$Z_p^{\{N\}}(\vec{\hat{x}}) =: \int_{-\pi}^{\pi} \frac{dt}{2\pi} \exp\left[\sum_{n=1}^{N} \frac{1}{2}(\hat{x}_n \mathrm{e}^{\mathrm{i}nt} - \mathrm{H.c.}) - \mathrm{i}pt\right] : . \tag{6}$$

Here colons imply normal ordering and $\{N\} = 1, 2, \ldots, N$. The Z functions [30] [defined via Eq. (6)] are multidimensional generalizations of Bessel functions, analytically continued for complex arguments [37,38].

Setting the detuning to zero for simplicity, the DTTS with period $2\pi/\omega_J = 2\pi/(p\omega_1)$ manifests as a discrete rotational symmetry in the rotating frame [11,39,40],

$$\mathcal{R}(2\pi/p)\hat{H}_{\mathrm{RWA}} = \hat{H}_{\mathrm{RWA}}, \tag{7}$$

where $\mathcal{R}(\theta)\bullet = \hat{r}(\theta)\bullet\hat{r}^\dagger(\theta)$ with the operator $\hat{r}(\theta) = \exp(\mathrm{i}\theta\sum n\hat{a}_n^\dagger\hat{a}_n)$ rotating a state by an angle θ. The modes can be grouped according to their eigenvalue $\exp(k\mathrm{i}2\pi/p)$ when acted on by $\mathcal{R}(2\pi/p)$. The resonant harmonics all have $k = 0$; the other modes have $k \neq 0$ and fall into sets defined by

$$\vec{s}_k = (\hat{a}_k, \hat{a}_{p-k}^\dagger, \hat{a}_{p+k}, \hat{a}_{2p-k}^\dagger, \hat{a}_{2p+k}, \hat{a}_{3p-k}^\dagger, \ldots). \tag{8}$$

The number of distinct sets is $(p-1)/2$ for odd p, and $p/2$ for even.

To obtain critical couplings for continuous transitions in the classical regime, we employ the corresponding coherent state ansatz Hamiltonian obtained from Eq. (5), $\mathcal{H}_{\mathrm{RWA}}$. The fixed point corresponding to the symmetry-conserving solution is found and the critical drive strength, λ_c, at which this point becomes unstable, is identified using linear stability analysis; a detailed description of the method is given in Appendix B. Comparison with numerical integration [see Fig. 2(b)] demonstrates that this approach can identify the critical coupling accurately.

Despite the potential complexity of the problem, the linear stability analysis proves tractable for a wide choice of N and p. The fact that we only need to find the fixed points below the transition represents a significant simplification since, in this regime, only a subset of the modes (the resonant harmonics) have nonzero amplitudes, reducing the effective dimensionality of the problem. Furthermore, once obtained, the fixed point amplitudes for a given set of resonant harmonics can be applied to any combination of (p, N) with the same number of resonant harmonics via a simple scaling. We located fixed points for sets of up to nine resonant harmonics, which is sufficient for all combinations of N and p such that $N < 10p$. Finally, the special function form of the Hamiltonian [Eq. (5)] is readily differentiated, facilitating the calculation of the Jacobian matrix used for the stability analysis [30].

The stability is assessed by calculating whether small deviations from the fixed point shrink (stable) or grow (unstable). This is done by calculating the Jacobian matrix (a matrix of all possible $\partial\dot{\alpha}_n/\partial\alpha_m$) and seeing if it has any positive eigenvalues (indicating instability). More details are provided in Appendix B. As well as yielding values of the critical couplings for continuous transitions, the approach also reveals *how* the transition occurs. Below the transition, the Jacobian is block diagonal: couplings only occur between modes with the same eigenvalue under discrete rotation, k. The continuous transition emerges as an instability of the zero amplitude fixed point within just one of the $k \neq 0$ blocks. Numerical integration shows that this instability then spreads progressively to modes with different k values. One can think of the blocks like adjacent dominoes: the stability of each domino is independent of the others, but an instability and subsequent symmetry breaking in one spreads to the others.

Figure 3 shows how the threshold for a continuous transition depends on both N and p. The basic trend is of a critical drive strength that increases with mode number N (note $\lambda_c/\sqrt{N}$ is plotted). Even though all the modes are coupled to the Josephson drive, only one is resonant, hence it is not surprising that the transition typically becomes harder to reach as more modes are added. However, the nonlinear couplings between the modes enable a complex range of frequency conversion processes mediated by the drive, with new ones enabled with each mode added. Understanding these processes is key to understanding the complex interplay

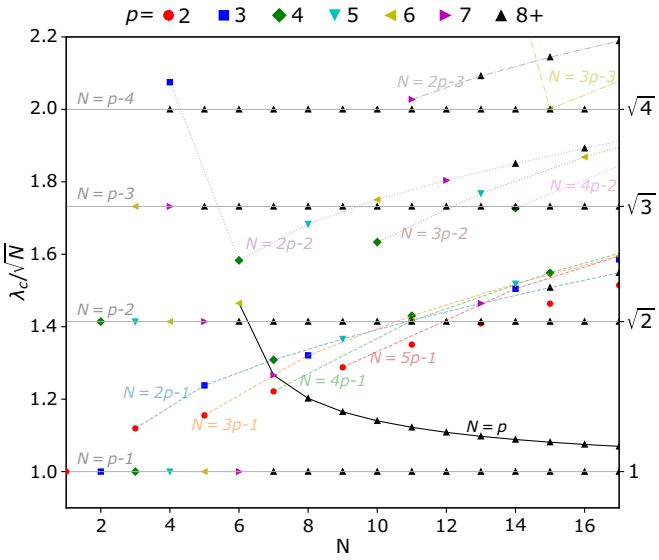

FIG. 3. Critical drive strength, λ_c at which a continuous transition takes place for a range of N and p values, calculated using linear stability analysis (detailed in Appendix B). Lines connect points with a specific relationship between N and p (labeled in each case).

between the behavior of λ_c and the precise relationship between N and p revealed in Fig. 3.

Qualitatively different trends emerge for $p/2 \leqslant N < p$, $N = p$, and $N > p$, which we consider in turn. Note that no continuous transition is possible for $N < p/2$. In this case, the lowest order processes are cubic or higher (creating three or more photons), and do not lead to continuous transitions [9,11].

For $p/2 < N < p$, an instability occurs via a parametric downconversion process in which the Josephson drive excites two modes whose frequencies sum to $\omega_J = p\omega_1$ [41]. The different blocks in the Jacobian, corresponding to different values of k, couple the pairs of modes ω_k and ω_{p-k}; in each case, the interaction is equivalent to that in a parametric amplifier (typically nondegenerate). The blocks differ only by factors of $\Delta_n = \Delta_1/\sqrt{n}$ (this scaling follows directly from the fact that the modes are harmonics of a microwave cavity with $\omega_n = n\omega_1$ [29]), with the parametric terms in block k proportional to $\Delta_k\Delta_{p-k}$. Since $\Delta_1\Delta_{p-1} > \Delta_2\Delta_{p-2} > \Delta_3\Delta_{p-3}...$ the most strongly excited parametric process involves the last mode added, ω_N, and one finds $\lambda_c = \sqrt{N(p-N)}$, leading to the horizontal lines in Fig. 3. They form a ladder: keeping p fixed and increasing N moves us down the rungs. [Derivations of the expressions for λ_c given in this section are provided in Appendix B.]

The second regime is $N = p$, where the system now possesses a resonant mode and the critical coupling follows the solid black curve sloping downward in Fig. 3. The presence of a resonant mode impedes the transition by diverting energy away from the dominant parametric terms that now have a reduced coupling strength in the Jacobian. The critical drive is found to be $\lambda_c = \sqrt{p-1}/[2J_1'(x)]$, with $J_1(x)$ a Bessel function and x the fixed point amplitude of the resonant mode multiplied by $2\Delta_p$, which satisfies [21] $x^2 = (4\lambda/p)J_1(x)$.

The impeding effect of the resonant mode is strongest at low p values. For $p = N < 6$, no continuous transition occurs at all, but as p is increased the impact of the resonant mode gets weaker and a simpler approximate relation can be derived, $\lambda_c \approx p\sqrt{p-1}/(p-3/2)$, for large p. Eventually, λ_c tends to $\sqrt{N}$, matching the critical drive for $N = p-1$, in the $p \to \infty$ limit.

Finally, we consider cases where $N > p$. The number of resonant harmonics grows with N, making it progressively more difficult to obtain the below-transition fixed point. Further complexity is introduced by an increase in the number of modes within each block beyond two, enabling beam-splitter-type interactions in which modes with frequency *difference* a multiple of $\omega_J = p\omega_1$ exchange energy with each other mediated by the drive and the resonant harmonics. Nevertheless, the blocks with different k remain fundamentally the same as one another, differing only by factors of Δ_n and by how they are truncated by the finite mode number.

In this regime, it is helpful to think about the processes enabled by the last mode added: relatively low values of λ_c are found where this mode enables additional parametric processes in which two modes can jointly be excited. The best examples occur when $N = qp - 1$ for $q = 2, 3...$—in each such case, the Nth mode is added to the $k = 1$ space and is parametrically coupled to the fundamental: these modes can be excited together by combinations of the drive and the resonant harmonics ($\omega_1 + \omega_N = qp\omega_1$). Similar effects arise when $N = qp - 2$, $N = qp - 3$, etc., with the Nth mode adding a new parametric process to the $k = 2, 3, \ldots$ space. But as $\Delta_1\Delta_{qp-1} > \Delta_2\Delta_{qp-2} > \Delta_3\Delta_{qp-3}$, the new process added gets weaker with increasing k and the corresponding value of λ_c increases (similar to the ladder seen for $N < p$). From this, it follows that for $N = qp - k$ and $k \leqslant (p/2)$ any continuous DTTSB is in subspace k.

V. DISCONTINUOUS TRANSITIONS

We now examine the drive at which the DTTS breaking transition actually occurs in a given system, λ_{sb}, which need not necessarily correspond to λ_c since a *discontinuous* transition is also possible (see Fig. 2). Discontinuous transitions have to be identified via numerical integration by tracing how the symmetry-broken state evolves as the drive strength is lowered progressively.

Combining numerical integration data with the critical drives we previously obtained for continuous transitions, Fig. 4 shows the value of λ_{sb} as a function of N for $p = 2$, 3, and 4. The basic message is that the N and p values that we identified as leading to a relatively small λ_c (i.e., within the range shown in Fig. 3), a continuous transition does indeed occur before any discontinuous one is reached, but where a continuous transition requires a relatively large drive strength it will generally be forestalled by a discontinuous one. Specifically, the relatively low values of λ_c that arise for $N = qp - 1$ (with $q = 2, 3, \ldots$) facilitate continuous transitions at a value of λ_{sb} significantly lower than neighboring discontinuous transitions in each case. These are, in fact, the only continuous transitions that occur for $p = 2$ and $p = 3$, which only possess blocks with $k = 0$ and 1. For $p = 4$, which also has a $k = 2$ block, continuous transitions occur when $N = 4q - 2$

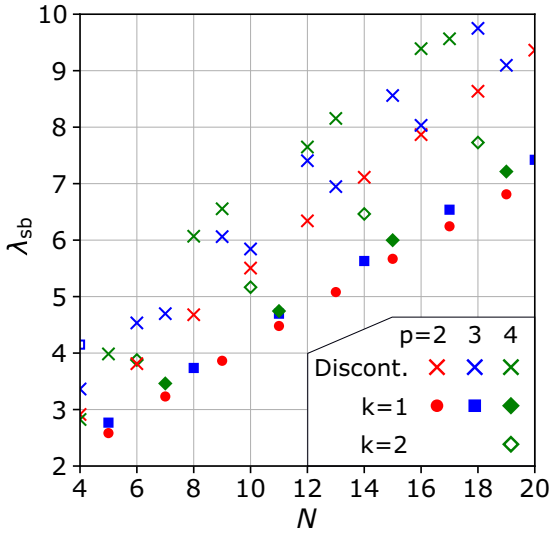

FIG. 4. Drive at which a DTTS breaking transition occurs in a given system, λ_{sb}, as a function of N for $p = 2, 3, 4$. Crosses: Discontinuous transitions. Solid (hollow) points: Continuous transitions originating within the $k = 1$ ($k = 2$) block.

(triggered within the $k = 2$ block) as well as when $N = 4q - 1$ (triggered in the $k = 1$ block).

VI. CONCLUSIONS

The transition in a many-mode JJ-cavity system that breaks the DTTS of the Hamiltonian occurs either continuously or discontinuously as a function of the system parameters. We developed an approximate classical description of the system dynamics that enabled us to determine when a continuous transition occurs efficiently, leading to simple analytic expressions in some cases. We also examined exactly how these transitions occur: they involve an instability within a particular subset of modes linked by a symmetry property. This uncovered the existence of magic combinations of Josephson frequency and mode number which facilitate continuous transitions at relatively low drive strengths. In systems that do not match one of these combinations, the DTTS breaking transition is instead found to occur discontinuously at a relatively high drive strength.

Although we have assumed a sharp cutoff in the number of modes, we expect that our analysis will be relevant more generally in cases where the cutoff is soft (determined, e.g., by damping which increases smoothly with the mode number). In particular, we find that a change from a continuous to a discontinuous DTTS breaking transition can occur when the *effective* mode number (controlled by the details of the soft cutoff) is changed and that the tools used to understand the locations of the continuous transitions in Sec. IV retain an important role in explaining the behavior when the cutoff is no longer hard (see Appendix C for details).

Beyond the insights that our analysis gives into the complex and unusual classical dynamics of the JJL, it opens the way for a quantum analysis of the system which would reveal the extent to which couplings within each block might give rise to patterns of many-body entanglement and the extent to which quantum effects influence the location and nature of the DTTS breaking transition. Finally, we note that our approach could be adapted to describe a range of other nonlinear multimode circuit-QED systems driven in different ways, e.g., by an ac flux bias [2].

ACKNOWLEDGMENT

The work was supported by a Leverhulme Trust Research Project Grant (No. RBG-2018-213).

APPENDIX A: NUMERICAL INTEGRATION OF CLASSICAL EQUATIONS

Classical equations of motion are obtained using the coherent state ansatz. All of the modes are assumed to always be in coherent states with corresponding time-dependent amplitudes, $\{\alpha_l\}$. Normally ordering the Hamiltonian, one finds that these obey the following set of equations of motion [30]:

$$\dot{\alpha}_l(t) = -\frac{\mathrm{i}}{\hbar}\frac{\partial \mathcal{H}(t,\vec{\alpha})}{\partial \alpha_l^*} - \frac{\gamma}{2}\alpha_l(t), \tag{A1}$$

with the classical Hamiltonian

$$\mathcal{H}(t,\vec{\alpha}) = \sum_{n=1}^{N} \hbar\omega_n |\alpha_n|^2 - \tilde{E}_J \cos\left[\omega_J t + \sum_{n=1}^{N} 2\Delta_n \mathrm{Re}[\alpha_n]\right], \tag{A2}$$

where $\tilde{E}_J = E_J \exp[-\sum_{n=1}^{N} \Delta_n^2/2]$.

The coupled system of equations Eq. (A1) is solved numerically, using standard routines, to study the transition to the symmetry broken state. The principal difficulty lies in identifying the location of discontinuous transitions, as in such cases the emergence of a (stable) symmetry broken fixed point is accompanied by the coexistence of a stable symmetry preserving one. Our approach is to start by identifying the symmetry-broken fixed point well above the transition and seeking to follow it until it eventually disappears as the drive strength is reduced. Specifically, we begin with a random initial condition and a large λ value and evolve in time until the system has relaxed to a steady state with period $T = 2\pi/\omega_1$. This final state is then used as the initial condition for the next calculation at a slightly lower λ, and so on progressively until the period T disappears. We extract the component of α_n oscillating at ω_n by evaluating $\tilde{\alpha}_n = \int_0^{10T} (dt/10T)\alpha_n(t)\exp(\mathrm{i}\omega_n t)$.

The discontinuous transition thresholds shown in Fig. 3 are found using this approach. As there were many such calculations, we used additional techniques to save computer resources. This consisted of a first-sweep calculation with large λ increments and a relatively large $\gamma/\omega_1 = 3 \times 10^{-2}$ to accelerate the convergence to a steady state. The point where the nonresonant modes become inactive with lowering λ is identified in this first sweep and a second sweep is carried out in this region. This second sweep used $\gamma/\omega_1 = 1 \times 10^{-2}$ and made use of a steady state from the previous sweep as the initial condition.

APPENDIX B: ANALYSIS OF CONTINUOUS TRANSITIONS

In this Appendix, we detail the methods used to identify the locations of continuous transitions. The first steps (described in Sec. IV) are a unitary transformation of the Hamiltonian (moving to a rotating frame) and a RWA. We then obtain the classical equations of motion by applying the coherent state ansatz to the RWA Hamiltonian [Eq. (5)]. Assuming that the detunings are all set to zero, this leads to the following equations of motion [30]:

$$\begin{aligned}\dot{\alpha}_l &= -\frac{\mathrm{i}}{\hbar}\frac{\partial \mathcal{H}_{\mathrm{RWA}}(\vec{\alpha})}{\partial \alpha_l^*} - \frac{\gamma}{2}\alpha_l \\ &= -\frac{\Delta_l \lambda \gamma}{2\Delta_1^2}\left[Z_{p+l}^{\{N\}}(2\mathrm{i}\vec{\Delta}\circ\vec{\alpha}) - Z_{p-l}^{\{N\}}(-2\mathrm{i}\vec{\Delta}\circ\vec{\alpha}^*)\right] - \frac{\gamma}{2}\alpha_l,\end{aligned} \tag{B1}$$

where the classical RWA Hamiltonian takes the form

$$\mathcal{H}_{\mathrm{RWA}}(\vec{\alpha}) = -\frac{\tilde{E}_J}{2}\left[Z_p^{\{N\}}(2\mathrm{i}\vec{\Delta}\circ\vec{\alpha}) + \mathrm{H.c.}\right]. \tag{B2}$$

Here we have adopted the vector notation so $\vec{\Delta} = (\Delta_1, \Delta_2, \ldots, \Delta_N)$ and $\vec{\alpha} = (\alpha_1, \alpha_2, \ldots, \alpha_N)$; the symbol $\circ$ indicates an elementwise product, i.e., $\vec{c} = \vec{a}\circ\vec{b}$ implies that $c_n = a_n b_n$. The Z functions are defined in the main text [Eq. (6)] and their properties (including differentiation) are discussed in detail in Ref. [30].

To obtain the critical drive strength for a continuous transition, we need to identify the nonzero amplitudes at the symmetry preserving fixed point (i.e., those of the resonant harmonics) and then determine the eigenvalues of the associated Jacobian. We address these in turn below (Appendices B 1 and B 2), after which we turn to examine the different uncoupled symmetry blocks that describe the system's dynamics in this regime (Appendix B 3). The symmetry blocks simplify the problem enough to allow analytic solutions in some cases, described in Appendix B 4.

1. Symmetry-preserving fixed point

Prior to a continuous transition, only resonant harmonics (i.e., modes at integer multiples of the drive frequency) are excited; the others have zero amplitude. This makes finding a fixed point much easier as we can neglect all the inactive modes, working instead within a reduced mode space that includes just the resonant harmonics. When $pM \leqslant N < p(M+1)$, the N modes contain M resonant harmonics, this means we can simply replace $Z_p^{1,2,\ldots,N}$ by $Z_p^{p,2p,\ldots,Mp}$ in Eq. (B1).

Furthermore, a simple rescaling allows us to map the problem onto one which only depends on the number of resonant harmonics, M, but is independent of the choice of p. The mapping relabels the mode index for the resonant harmonics $n \to n'$, where n' runs from 1 to M, and $p \to p' = 1$, using the identity [30] $Z_p^{p,2p,\ldots,Mp} = Z_1^{1,2,\ldots,M}$. The values of the zero-point uncertainties and mode amplitudes also need to be rescaled, since mode n' in the reduced space refers to mode $n = pn'$ in the full space, $\Delta'_{n'} = \Delta_{pn'} = \Delta_n/\sqrt{p}$. The mode amplitudes undergo the opposite scaling so $\Delta'_{n'}\alpha'_{n'} = \Delta_{pn'}\alpha_{pn'}$. The dimensionless drive, λ, remains unchanged.

The point of this rescaling is that once a solution is found for a given value of M, it can be used to describe the below-transition mode amplitudes of any situation with the same number of resonant harmonics [i.e., where $pM \leqslant N < p(M+1)$]. We carried out nine fixed point calculations [30], with M from 1 to 9. These provide the fixed points needed to describe the below-transition dynamics for any N, p such that $N < 10p$. In finding these fixed points, we are helped by the fact that for $\lambda = 0$ all modes have zero amplitude and that at each step, as λ is incremented higher, the new fixed point is located near the previous one, which was used as the solver's initial guess. At each stage, we located the fixed points by evaluating the Z functions using the integral definitions [Eq. (5)] and varying the values of the amplitudes in small increments away from the previous fixed point.

The behavior of the resonant harmonic fixed points has two stages: First, a phase-locked regime in which the complex mode amplitudes $\alpha'_n = A'_n \exp(i\theta'_n)$ have phases that remain fixed at $\theta'_m = (1-m)\pi/2$. Here only the moduli $A'_n = |\alpha'_n|$ change with λ. At high λ, this regime ends in a bifurcation, after which the mode phases change with λ and the problem becomes more difficult to solve. The $M = 1$ case of this bifurcation is described in Ref. [21]. We tracked the fixed point amplitudes as a function of λ for each of the resonant harmonics up to this bifurcation.

2. Jacobian

The stability of the symmetry preserving fixed point is determined by the corresponding Jacobian matrix, $\bar{J}$. Casting the equations of motion Eq. (B1) in the compact form $\dot{\vec{\alpha}} = \vec{f}(\vec{\alpha}, \vec{\Delta}, \lambda, \gamma)$, the Jacobian is defined as

$$\bar{J}^T = \begin{pmatrix} \frac{\partial}{\partial\alpha_1} & \frac{\partial}{\partial\alpha_1^*} & \frac{\partial}{\partial\alpha_2} & \frac{\partial}{\partial\alpha_2^*}\ldots \end{pmatrix}^T \begin{pmatrix} f_1 & f_1^* & f_2 & f_2^*\ldots \end{pmatrix}. \tag{B3}$$

The necessary derivatives can be evaluated straightforwardly [30], and we find

$$\frac{\partial f_j}{\partial \alpha_l} = -i\Delta_j\Delta_l G_{j-l} - \frac{\gamma}{2}\delta_{l,j}, \tag{B4}$$

where we have defined

$$G_n = -\frac{\tilde{E}_J}{2\hbar}\left[Z_{p+n}^{\{N\}}(2\mathrm{i}\vec{\Delta}\circ\vec{\alpha}) + Z_{p-n}^{\{N\}}(-2\mathrm{i}\vec{\Delta}\circ\vec{\alpha}^*)\right], \tag{B5}$$

with $\vec{\alpha}$ taking the corresponding fixed point value. G_n does *not* appear in the fixed point expression, Eq. (B1), as the latter has a minus sign between the Z functions.

The Jacobian is relatively sparse, with most elements zero in the symmetry-preserving state: $G_n = 0$ except when $n = 0, \pm p, \pm 2p\ldots$. Where G_n is nonzero, it can be expressed using Z functions with dimension M using the same mode reduction procedure as before.

3. Block diagonal structure

The Jacobian matrix can be rearranged so it takes a block diagonal form. The first stage involves separating out the terms that correspond to the resonant harmonics: Formally, we can write the Jacobian as $\bar{J} = \bar{J}_{\mathrm{NH}} \oplus \bar{J}_{\mathrm{H}}$, where $\bar{J}_{\mathrm{H(NH)}}$ is

a matrix of size $2M$ $[2(N-M)]$ squared, involving just the modes that are (not) resonant harmonics of $\omega_d = p\omega_1$; the direct sum ($\oplus$) notation builds the full Jacobian by placing the component block matrices corner to corner.

We can also carry out a simple reordering of the rows/columns to bring $\overline{J}_{\rm NH}$ into a block diagonal form. These blocks are indexed by k, which labels the rotational symmetry subspace and runs from 1 to $(p-1)/2$ for p odd and to $p/2$ for p even. Block k involves the modes (k, $p-k$, $p+k$, $2p-k$, $2p+k$, $3p-k$,...) terminating the sequence as appropriate given the number of modes N [see Eqs. (7) and (8) in the main text], and takes the form

$$\overline{J}_k = \begin{pmatrix} \frac{\partial f_k}{\partial \alpha_k} & \frac{\partial f_k}{\partial \alpha^*_{p-k}} & \\ \frac{\partial f^*_{p-k}}{\partial \alpha_k} & \frac{\partial f^*_{p-k}}{\partial \alpha^*_{p-k}} & \\ & & \ddots \end{pmatrix} = \mathrm{i}\,\overline{\Delta}_k \begin{pmatrix} -G_0 & -G_{+p} & \\ +G_{-p} & +G_0 & \\ & & \ddots \end{pmatrix} \overline{\Delta}_k - (\gamma/2)\mathbb{I}, \tag{B6}$$

where $\overline{\Delta}_k$ is a diagonal matrix with elements Δ_k, Δ_{p-k}, ... For odd p, the block of the Jacobian for modes which aren't resonant harmonics, $\overline{J}_{\rm NH}$, consists of a direct sum of the $(p-1)/2$ different $k \neq 0$ blocks, $\overline{J}_k$, together with their complex conjugates, $\overline{J}^*_k$,

$$\overline{J}_{\rm NH} = \bigoplus_{k=1}^{(p-1)/2} (\overline{J}_k \oplus \overline{J}^*_k). \tag{B7}$$

For even p, things are slightly more complicated as the block with $k = p/2$ is its own complex conjugate (it is similar to the band-edge mode in a crystal that lacks a counter propagating partner), and in this case

$$\overline{J}_{\rm NH} = \left[\bigoplus_{k=1}^{(p-1)/2} (\overline{J}_k \oplus \overline{J}^*_k) \right] \oplus \overline{J}_{p/2}. \tag{B8}$$

A continuous DTTSB transition occurs when an eigenvalue with a positive real part emerges in one of the $\overline{J}_k$ blocks within $\overline{J}_{\rm NH}$. Once a subspace has developed an instability, the fixed point changes as amplitudes of the modes in that space become nonzero. These nonzero amplitudes can generate new couplings, breaking the strict division into symmetry sectors and affecting the amplitudes of modes which were originally in different blocks. This mechanism allows the instability to propagate from a single block to affect all the modes in all the blocks.

We searched for the critical λ value at which an instability first occurs in $\overline{J}$ for a wide range of N and p. The corresponding k value of the unstable block is shown in Fig. 5. If the symmetry subspace of the instability is $k \neq 0$, then a continuous DTTSB transition can be identified. However, when the instability occurs in the $k = 0$ space, the instability does not represent a DTTSB transition but instead a bifurcation within the resonant harmonics. We did not identify the behavior of the resonant harmonics beyond the first bifurcation that they undergo and hence did not locate any continuous DTTSB transition in these cases.

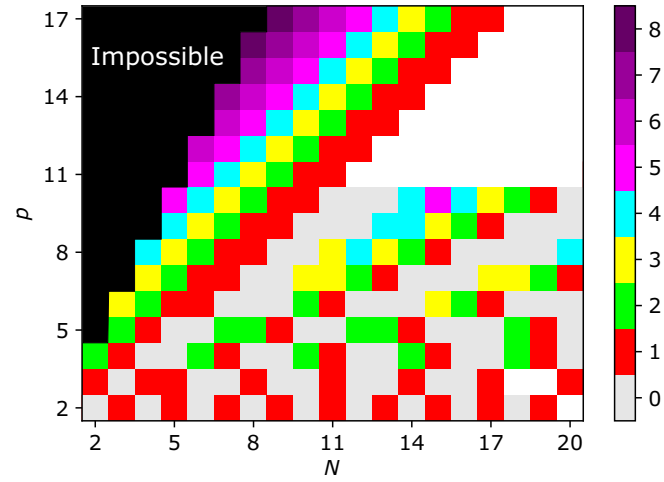

FIG. 5. Symmetry subspace, k, in which a continuous DTTSB transition emerges as a function of N and p. Gray indicates no DTTSB transition was found because an instability in the $k = 0$ space occurred first. White indicates an (N, p) combination that wasn't explored and black corresponds to cases where no transition is possible (see Appendix B 4).

4. Critical drive strengths in the few-mode regime: $N \leqslant p$

When $N \leqslant p$, the form of the Jacobian matrix, $\overline{J}$, is particularly simple, with each $\overline{J}_k$ taking the form of a 2×2 matrix that allows analytic results to be derived. One finds that for $\Delta_n = \Delta_1/\sqrt{n}$, the first instability occurs in the $k = p - N$ subspace for $N < p$ or $k = 1$ when $N = p$, with a critical drive given by

$$\lambda_{\rm c} = \frac{\tilde{E}_J \Delta_1^2}{\hbar\gamma} = \begin{cases} \infty & 2N < p \\ \sqrt{N(p-N)} & N < p \leqslant 2N \\ \frac{\sqrt{p-1}}{2J_1(2\Delta_p A_p)} & N = p. \end{cases} \tag{B9}$$

A continuous transition, occurring via a pitchfork bifurcation, is only possible in the presence of a quadratic term in the Hamiltonian [9,11]. This means that when the lowest order energy-conserving processes produce three or more photons, only discontinuous transitions are possible. Hence, the first line of Eq. (B9): No continuous transition is possible if the drive frequency is more than twice that of the highest frequency mode.

For $N = p$ (a single resonant harmonic), we can derive a simpler expression for λ_c assuming $p \gg 1$ and $\Delta_1 A_p/\sqrt{p} \ll 1$. Substituting Eq. (B9) into the fixed point expression [21], $\tilde{E}_J/(\hbar\gamma) = A_p^2/J_1(2\Delta_p A_p)$, provides an approximate equation for the amplitude of the resonant harmonic at the instability $\Delta_1 A_p \simeq 2$. Substituting this back into Eq. (B9) then leads to the relation $\lambda_{\rm c} \approx p\sqrt{p-1}/(p-3/2)$. This approximation proves quite accurate for $p > 10$.

APPENDIX C: SOFT CUTOFF

The assumption that all modes share a common decay rate, γ, is an idealization. The damping rates of each mode in any real device will be unequal and depend on the details of the design/geometry [42]. For a coplanar microwave cavity, the

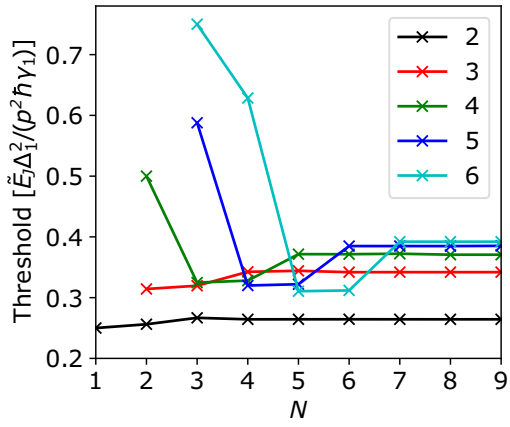

FIG. 6. Threshold value $\lambda_{\rm th} = \tilde{E}_J\Delta_1^2/(p^2\hbar\gamma_1)$ at which the symmetry unbroken solution becomes unstable with $p = 2, 3, 4, 5, 6$, $\gamma_n = n^2\gamma_1$ and $\Delta_n = \Delta_1/\sqrt{n}$. Note that $\lambda_{\rm th}$ is defined in terms of $p^2\gamma_1 = \gamma_p$ rather than just γ_1.

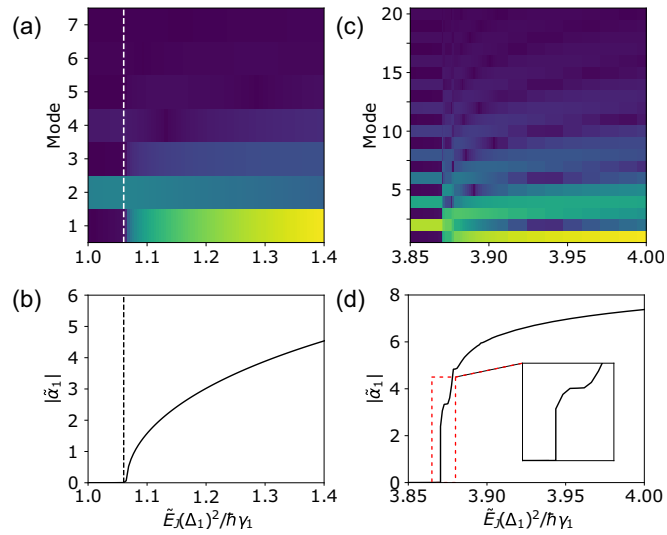

FIG. 7. Continuous and discontinuous transitions with soft cutoffs. The long-time behavior obtained from numerical integration of $|\tilde{\alpha}_n|^{1/2}$ (a),(c) and $|\tilde{\alpha}_1|$ (b),(d) is shown. In (a),(b) $\gamma_I = 0$ leading to a continuous transition, while in (c),(d) with $\gamma_I = 34\Gamma_E$ it is discontinuous. (a),(b) dashed line: analytic prediction from stability analysis (see Fig. 6) (d) inset: zoom-in of the step-like discontinuous transition. Note that the number of modes that play a role at the transition clearly increases as we go from (a) to (b). In both cases, we set $p = 2$.

modes have a loss of the form

$$\gamma_n = \gamma_I + \Gamma_E\, n^2, \tag{C1}$$

where γ_I describes internal losses and Γ_E external losses due to coupling to a nearby waveguide [29].

Equation (C1) implies three regimes. First, the undercoupled regime, $\Gamma_E/\gamma_I \to 0$, considered in the main paper. Second, the strongly overcoupled regime $\gamma_I/\Gamma_E \to 0$. Third, an intermediate regime where both components are nonzero. The following sections consider the overcoupled and intermediate cases in turn.

1. Overcoupled regime

Adjusting the fixed point Eq. (B1) and the Jacobian to study the overcoupled regime with $\gamma_n = n^2\gamma_1$ is straightforward. The thresholds for continuous transitions predicted within this model are shown in Fig. 6. The location of the threshold clearly saturates for large enough N, in contrast to the undercoupled regime discussed in the main paper. The quadratic increase in damping with mode number acts as a soft cutoff, naturally limiting the number of modes that affect a given threshold.

For $N < p$, the results in Fig. 6 qualitatively match those for constant loss, with more modes reducing the threshold by enabling stronger parametric processes. Unsurprisingly, the increased damping for the higher order modes reduces their impact. We see that additional modes past $N = p + 1$ have barely any effect on the threshold location, an effect which can be understood from the block structure of the modes. Mode $p - 1$ introduces a new (efficient) parametric process and thus strongly lowers the threshold. Mode p introduces the resonant mode which diverts energy from the nonresonant modes and raises the threshold (slightly). Then, mode $p + 1$ is in the all-important $k = 1$ block so it too can affect the dynamics of the transition. However, all modes between $p + 1$ and $2p - 1$ are in $k > 1$ blocks, so they cannot interact with the modes that drive the transition. This, combined with the quadratically ramping loss rate results in modes above $N = p + 1$ being essentially irrelevant.

For completeness, we note that when $p > 2$ the continuous transitions whose locations are shown Fig. 6, are preceded by discontinuous ones, so the threshold values plotted do not describe the first appearance of a symmetry broken state but instead the point beyond which there is no symmetry-unbroken state. Curiously, numerical integration finds discontinuous transitions at $\tilde{E}_J\Delta_1^2/(\hbar\gamma_1) \approx 2.2$, 3.3, 4.4, and 5.5 for $p = 3$, 4, 5, and 6 respectively.

Mathematically, we can adapt the method described in Appendix B 4 to cases where the loss changes as a power of n, $\gamma_n = n^l\gamma_1$, with $l \geqslant 0$. For $l = 0$, we have constant loss and $l = 2$ gives the quadratically increasing rates just discussed. For this class of loss relations, Eq. (B9) generalizes to

$$\lambda_c = \frac{\tilde{E}_J\Delta_1^2}{\hbar\gamma_1} = \begin{cases} \infty & 2N < p \\ [N(p-N)]^{(1+l)/2} & N < p \leqslant 2N \\ \frac{(p-1)^{(1+l)/2}}{2J_1'(2\Delta_p A_p)}. & N = p. \end{cases} \tag{C2}$$

In the limit $l \to \infty$, every mode except the first has an infinite damping rate and these expressions recover the results for $N = 1$. For large l, A_p tends to zero and thus $J_1'(2\Delta_p A_p)$ to $1/2$. For $p = 2$, the instability condition becomes $\tilde{E}_J\Delta_1^2/\gamma_1 = 1$, matching the known case of a single mode driven at twice its resonant frequency [21]. For $p > 2$ and $N = 1$, when $l \to \infty$ we recover the known result that the origin never becomes unstable (due to a rotational symmetry constraint in phase space [9,11]).

2. Intermediate coupling numerics

A striking feature of the hard-cutoff model is that transitions to the symmetry-broken state can be either continuous or discontinuous, depending on the location of the cutoff (i.e., the number of modes, N). In the following, we show that the appearance of both continuous and discontinuous transitions is not simply an artifact of the hard cutoff and that one can move from one to the other by tuning the location of a soft cutoff.

For a soft cutoff, the number of modes that are relevant for a given p depends on the ratio γ_I/Γ_E [see Eq. (C1)]. Figure 7 illustrates how changing the ratio γ_I/Γ_E (from 0 to 34) changes the number of modes that play a role in the $p = 2$ transition (analogous to changing N for the hard cutoff). In the $\gamma_I = 0$ case, a continuous transition takes place (at the location predicted by the stability analysis). However, for $\gamma_I = 34\Gamma_E$ the transition is instead discontinuous. In each case, the numerical integrations included sufficient modes (10 and 29, respectively) to ensure the soft cutoff is significantly exceeded (i.e., we are in a regime where the results no longer change when further modes are added). Thus, the change from continuous to discontinuous transitions which occurs as N is varied for a hard cutoff is echoed by the possibility of changing between continuous and discontinuous transitions by tuning the effective number of modes for a soft cutoff.

[1] X. Gu, A. F. Kockum, A. Miranowicz, Y.-X. Liu, and F. Nori, Phys. Rep. **718-719**, 1 (2017).

[2] I.-M. Svensson, A. Bengtsson, P. Krantz, J. Bylander, V. Shumeiko, and P. Delsing, Phys. Rev. B **96**, 174503 (2017).

[3] C. W. Sandbo Chang, C. Sabín, P. Forn-Díaz, F. Quijandría, A. M. Vadiraj, I. Nsanzineza, G. Johansson, and C. M. Wilson, Phys. Rev. X **10**, 011011 (2020).

[4] M. Hofheinz, F. Portier, Q. Baudouin, P. Joyez, D. Vion, P. Bertet, P. Roche, and D. Esteve, Phys. Rev. Lett. **106**, 217005 (2011).

[5] M. Westig, B. Kubala, O. Parlavecchio, Y. Mukharsky, C. Altimiras, P. Joyez, D. Vion, P. Roche, D. Esteve, M. Hofheinz, M. Trif, P. Simon, J. Ankerhold, and F. Portier, Phys. Rev. Lett. **119**, 137001 (2017).

[6] A. Peugeot, G. Ménard, S. Dambach, M. Westig, B. Kubala, Y. Mukharsky, C. Altimiras, P. Joyez, D. Vion, P. Roche, D. Esteve, P. Milman, J. Leppäkangas, G. Johansson, M. Hofheinz, J. Ankerhold, and F. Portier, Phys. Rev. X **11**, 031008 (2021).

[7] G. C. Ménard, A. Peugeot, C. Padurariu, C. Rolland, B. Kubala, Y. Mukharsky, Z. Iftikhar, C. Altimiras, P. Roche, H. le Sueur, P. Joyez, D. Vion, D. Esteve, J. Ankerhold, and F. Portier, Phys. Rev. X **12**, 021006 (2022).

[8] J. Leppäkangas, G. Johansson, M. Marthaler, and M. Fogelström, Phys. Rev. Lett. **110**, 267004 (2013).

[9] Y. Zhang, J. Gosner, S. M. Girvin, J. Ankerhold, and M. I. Dykman, Phys. Rev. A **96**, 052124 (2017).

[10] J. Gosner, B. Kubala, and J. Ankerhold, Phys. Rev. B **101**, 054501 (2020).

[11] B. Lang and A. D. Armour, New J. Phys. **23**, 033021 (2021).

[12] L. Arndt and F. Hassler, Phys. Rev. Lett. **128**, 187701 (2022).

[13] M. I. Dykman, C. Bruder, N. Lörch, and Y. Zhang, Phys. Rev. B **98**, 195444 (2018).

[14] N. Y. Yao, C. Nayak, L. Balents, and M. P. Zaletel, Nat. Phys. **16**, 438 (2020).

[15] H. Keßler, J. G. Cosme, C. Georges, L. Mathey, and A. Hemmerich, New J. Phys. **22**, 085002 (2020).

[16] H. Keßler, P. Kongkhambut, C. Georges, L. Mathey, J. G. Cosme, and A. Hemmerich, Phys. Rev. Lett. **127**, 043602 (2021).

[17] T. L. Heugel, A. Eichler, R. Chitra, and O. Zilberberg, arXiv:2203.05577.

[18] S. Chakram, A. E. Oriani, R. K. Naik, A. V. Dixit, K. He, A. Agrawal, H. Kwon, and D. I. Schuster, Phys. Rev. Lett. **127**, 107701 (2021).

[19] M. C. Cassidy, A. Bruno, S. Rubbert, M. Irfan, J. Kammhuber, R. N. Schouten, A. R. Akhmerov, and L. P. Kouwenhoven, Science **355**, 939 (2017).

[20] S. H. Simon and N. R. Cooper, Phys. Rev. Lett. **121**, 027004 (2018).

[21] A. D. Armour, M. P. Blencowe, E. Brahimi, and A. J. Rimberg, Phys. Rev. Lett. **111**, 247001 (2013).

[22] A. D. Armour, B. Kubala, and J. Ankerhold, Phys. Rev. B **91**, 184508 (2015).

[23] F. Chen, J. Li, A. D. Armour, E. Brahimi, J. Stettenheim, A. J. Sirois, R. W. Simmonds, M. P. Blencowe, and A. J. Rimberg, Phys. Rev. B **90**, 020506(R) (2014).

[24] M. Trif and P. Simon, Phys. Rev. B **92**, 014503 (2015).

[25] P. P. Hofer, J.-R. Souquet, and A. A. Clerk, Phys. Rev. B **93**, 041418(R) (2016).

[26] S. Dambach, B. Kubala, and J. Ankerhold, New J. Phys. **19**, 023027 (2017).

[27] H. J. Carmichael, *Statistical Methods in Quantum Optics 1: Master Equations and Fokker-Planck Equations* (Springer-Verlag, Berlin 1999).

[28] B. Kubala, V. Gramich, and J. Ankerhold, Phys. Scr. **2015**, 014029 (2015).

[29] M. Göppl, A. Fragner, M. Baur, R. Bianchetti, S. Filipp, J. M. Fink, P. J. Leek, G. Puebla, L. Steffen, and A. Wallraff, J. Appl. Phys. **104**, 113904 (2008).

[30] K. Wood, A. D. Armour, and B. Lang, Phys. Rev. B **104**, 155424 (2021).

[31] H. J. Carmichael, Phys. Rev. X **5**, 031028 (2015).

[32] A. D. Armour, B. Kubala, and J. Ankerhold, Phys. Rev. B **96**, 214509 (2017).

[33] H. Grabert, G.-L. Ingold, and B. Paul, Europhys. Lett. **44**, 360 (1998).

[34] V. Gramich, B. Kubala, S. Rohrer, and J. Ankerhold, Phys. Rev. Lett. **111**, 247002 (2013).

[35] S. Léger, J. Puertas-Martínez, K. Bharadwaj, R. Dassonneville, J. Delaforce, F. Foroughi, V. Milchakov, L. Planat, O. Buisson, C. Naud, W. Hasch-Guichard, S. Florens, I. Snyman, and N. Roch, Nat. Commun. **10**, 5259 (2019).

[36] The RWA is expected to be a good approximation on-resonance provided $\gamma \ll \omega_n$ and $E_J\Delta_n \ll \omega_n$ for all n [30].

[37] G. Dattoli, A. Torre, and S. Lorenzutta, Le Matematiche **53**, 387 (1998).

[38] H. Korsch, A. Klumpp, and D. Witthaut, J. Phys. A: Math. Gen. **39**, 14947 (2006).

[39] L. Guo, M. Marthaler, and G. Schön, Phys. Rev. Lett. **111**, 205303 (2013).

[40] L. Guo and P. Liang, New J. Phys. **22**, 075003 (2020).

[41] When $p = 2N$ the Nth mode acts as a degenerate parametric amplifier whose instability drives a continuous transition.

[42] G. Aiello, *Quantum dynamics of a high impedance microwave cavity strongly coupled to a Josephson junction.*, Ph.D. thesis, Université Paris-Saclay, HAL archives-ouvertes, 2020.